Supplementary Information

Dipolar interaction-mediated molecular anchoring electrolyte enables wide-temperature sodium-ion batteries with enhanced safety and durability

Yong-Li Heng[1], Zhen-Yi Gu[1*], Yuan-Zheng Tang[2], Han-Hao Liu[3], Xiao-Tong Wang[1], Jie Wang[3], Shu-Yu Li[3], Xing-Long Wu[1*]

1 Y.-L. Heng, Z.-Y. Gu, X.-T. Wang, X.-L. Wu

State Key Laboratory of Integrated Optoelectronics, and MOE Key Laboratory for UV Light-Emitting Materials and Technology, Department of Physics, Northeast Normal University, Changchun, Jilin 130024, P. R. China

E-mail: guzy166@nenu.edu.cn; xinglong@nenu.edu.cn

2 Y.-Z. Tang

Qingdao University of Science and Technology, Qingdao, Shandong 260061, China

3 H.-H. Liu, J. Wang, S.-Y. Li

Department of Chemistry, Northeast Normal University, Changchun, Jilin 130024, P. R. China

Supplementary Note 1: Exploration of the sudden drop of cell capacity during the cycle.

The sudden decline in cell capacity was observed, particularly for the HC||NVPOF full cells with ND and NP electrolytes at 0.2 C and 50 ℃ after the 53th and 76th cycle, respectively (Fig. 5i). This phenomenon is very likely caused by the cell balancing or cell assembly issue, and does not represent the general electrochemical behaviors of the electrolyte systems. The conjecture was confirmed after rechecking several sets of parallel cycling data. Consequently, the abnormal end data points of 0 mAh g^{-1} for the ND and NP electrolyte curves were not presented in Fig. 5i.

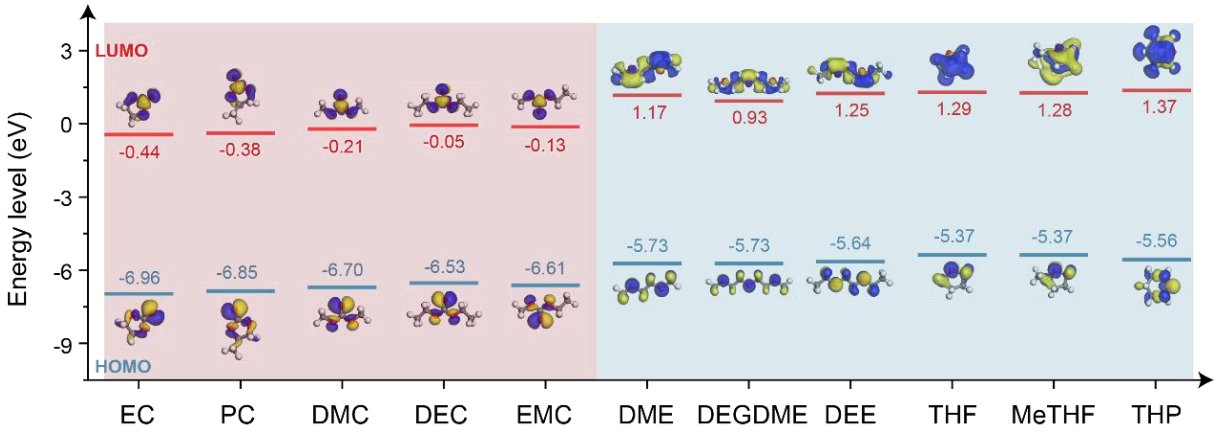

Supplementary Figure 1. The calculated HOMO/LUMO energy levels of a series of carbonate ester and ether based solvents. Colors of elements: H, white; C, grey; O, red.

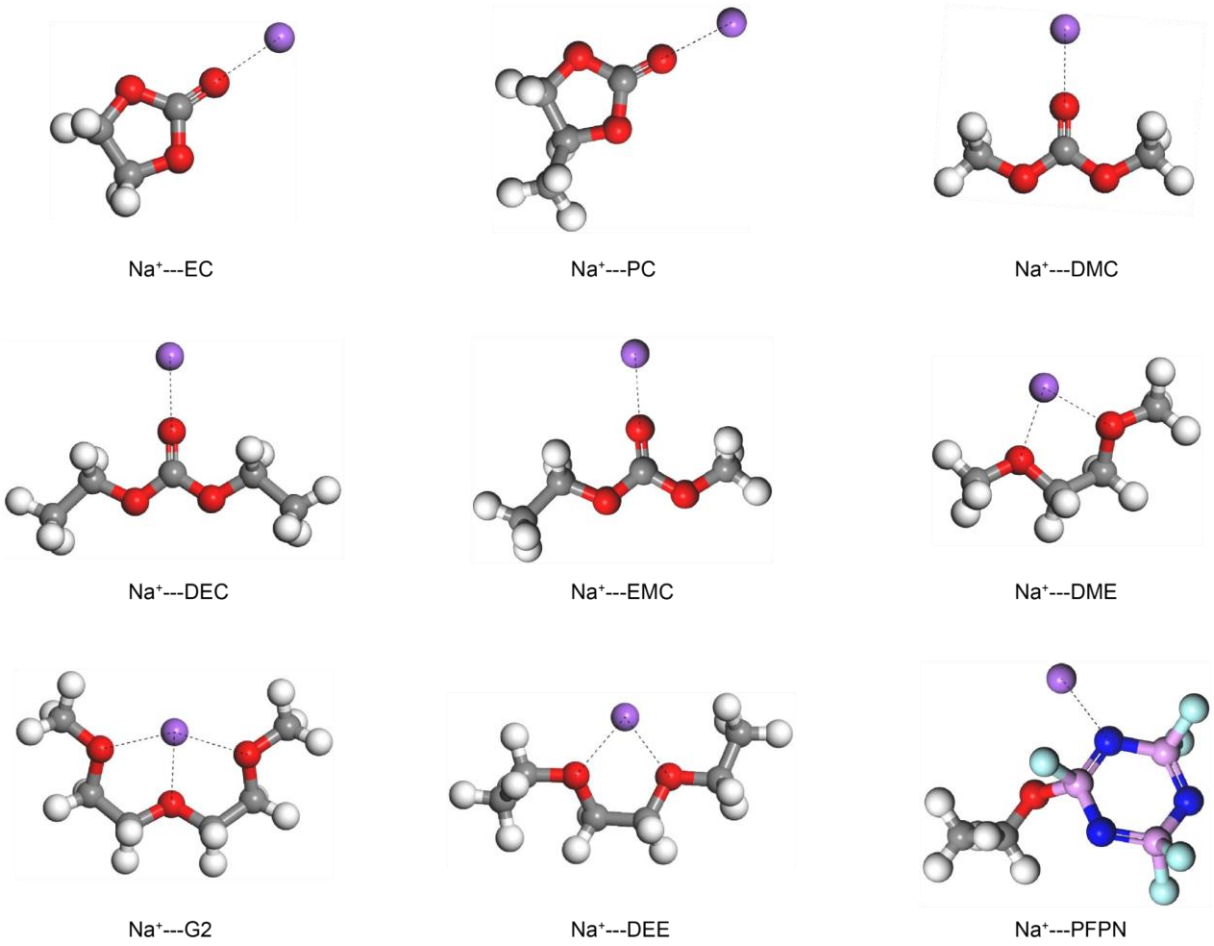

Supplementary Figure 2. The binding energy calculations with optimized structures for various Na^+-solvent complexes. Colors of elements: H, white; C, grey; N, blue; O, red; F, cyan; P, pink; Na, purple.

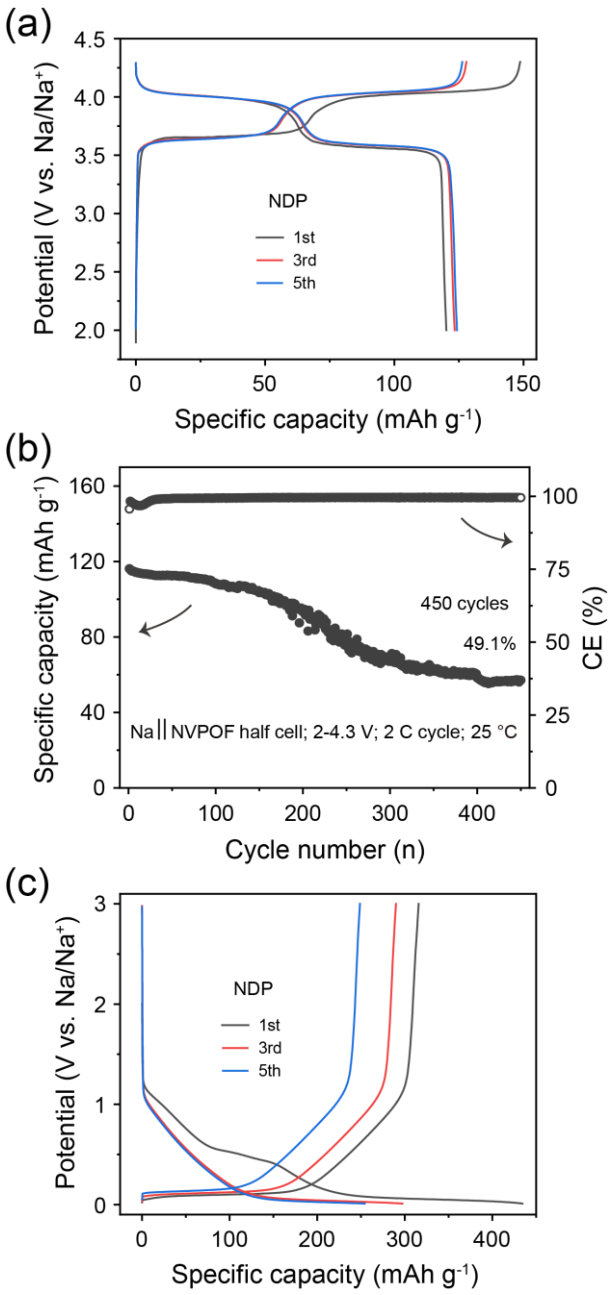

Supplementary Figure 3. (a) GCD curves of the sodium-ion half cells with NVPOF positive electrode at 0.1 C. (b) Cycling stability of Na||NVPOF half cells with NDP at 2 C. (c) GCD curves of the sodium-ion half cells with HC negative electrode at 25 mA g^{-1} in the NDP electrolyte.

By simply blending PC and DEE, the obtained NDP electrolyte exhibited unsatisfactory electrochemical stability with insufficient CEs for both NVPOF and HC electrodes, which may be attributed to the presence of abundant free solvents and the instability of electrode/electrolyte interfaces.

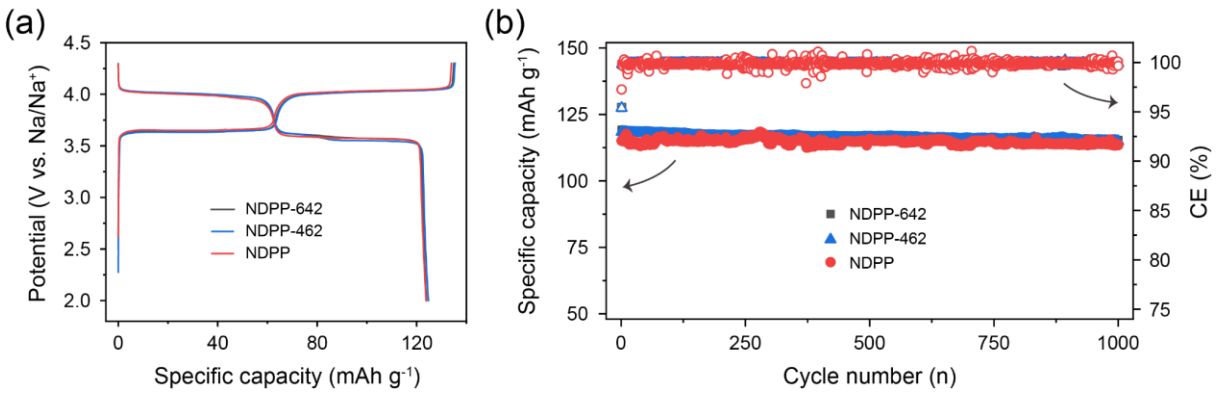

Supplementary Figure 4. Electrochemical investigations of the Na||NVPOF half cells with different NDPP-based electrolytes. (a) The first GCD curves at 0.1 C. (b) Cycling stability at 2 C.

The various integrated NDPP electrolytes have been prepared with different solvent ratios (DEE/PC = 4/6, 5/5, 6/4, in volume). Considering the weak salt solubility in PFPN, 0.8 M was chosen as an appropriate concentration. They all demonstrated the prominent electrochemical reversibility and stability, indicating the effectiveness of the dipolar interaction-mediated molecular anchoring engineering. The NDPP (0.8 M $NaPF_6$ in DEE-PC-PFPN, 5: 5: 2 in volume) sample was applied as a representative electrolyte model to further study the solvation and working mechanism.

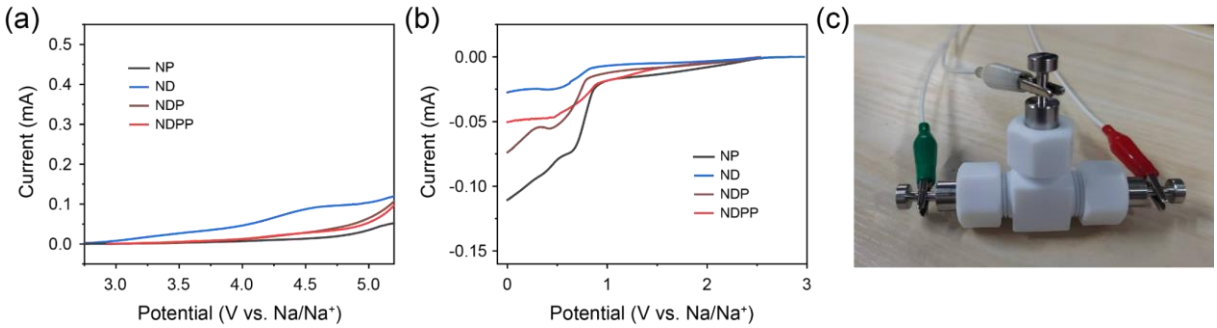

Supplementary Figure 5. Three-electrode LSV measurements of different electrolytes at 2 mV s^{-1}. (a) Electrochemical oxidation stability. (b) Electrochemical reduction stability. (c) Optical photograph of the three-electrode battery system.

Three-electrode cells with different electrolyte systems were assembled using stainless steel as the working electrode and sodium as the counter and reference electrodes. Similar to the two-electrode method, the sequence of electrochemical oxidation stability of these electrolytes is ND < NDP < NDPP < NP, while the sequence of their reduction stability is as follows: NP < NDP < NDPP < ND. Among them, the NDPP electrolyte demonstrates the comprehensive electrochemical stability to sustain the stable operation of the positive and negative electrodes. Despite the presence of complementary PC and DEE solvents, the NDP electrolyte fails to exhibit the desired electrochemical stability. This phenomenon further confirms the indispensable role of PFPN.

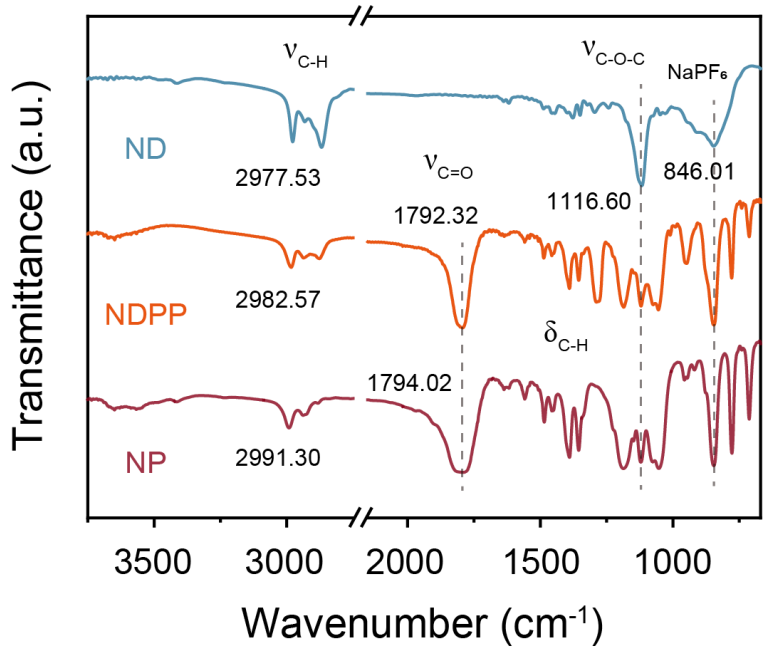

Supplementary Figure 6. The FTIR spectra of various electrolytes.

According to the FTIR spectra, the characteristic absorption peaks at 2800-3000 and 1350-1490 cm^{-1} correspond to the stretching and bending vibrations of C-H bonds in the solvents (PC, DEE, PFPN), respectively. The stretching vibrational peak of C=O in PC is observed at 1792.32 and 1794.02 cm^{-1} in NDPP and NP electrolytes, respectively, implying the reduced free PC solvent. The peak at 1116.60 cm^{-1} represents the C-O-C stretching vibration. The stronger vibrational peaks around 846.01 cm^{-1} are assigned to P-F bonds in PF_6^-. Additionally, the weak and broad absorption bands around 3500-3600 cm^{-1} can be attributed to the intermolecular hydrogen bond interactions.

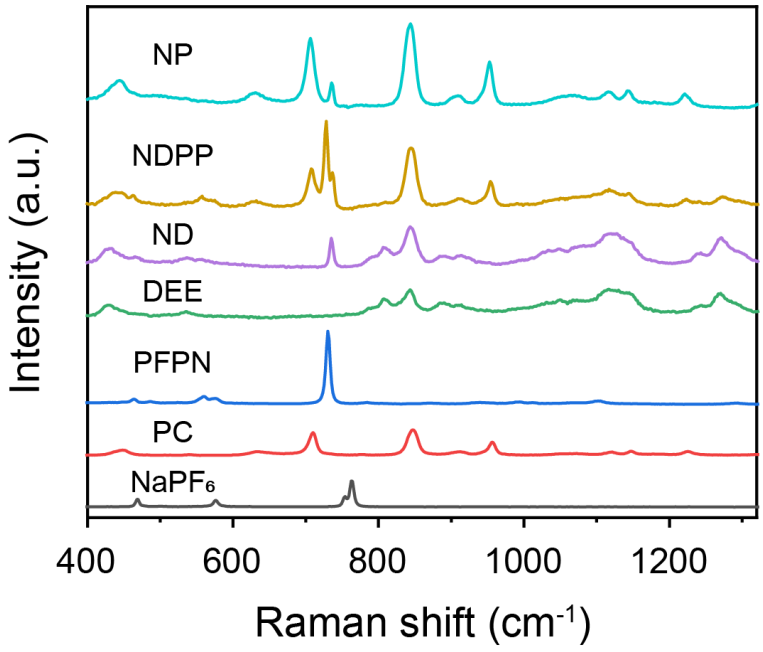

Supplementary Figure 7. Raman spectra of different electrolyte components.

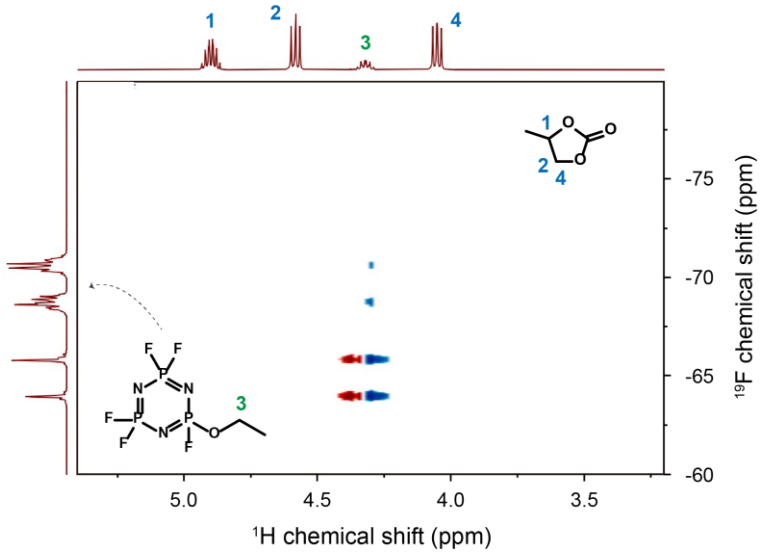

Supplementary Figure 8. The 2 D ^{1}H-^{19}F HOESY spectra of the PC/PFPN mixture.

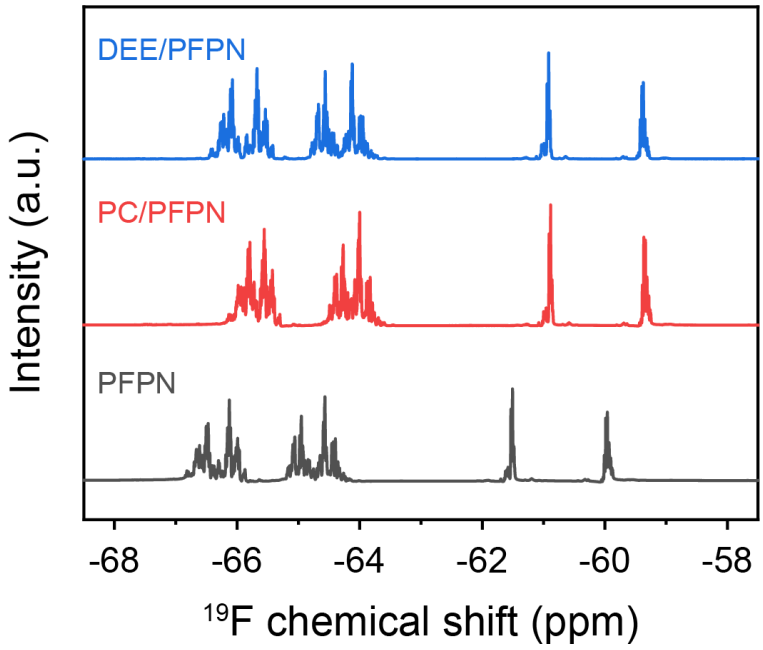

Supplementary Figure 9. ^{19}F NMR spectra of the pure PFPN, PC/PFPN and DEE/PFPN mixtures.

Compared to DEE/PFPN, the more obvious peak shift occurs in the PC/PFPN, indicating the stronger interaction between PC and PFPN.

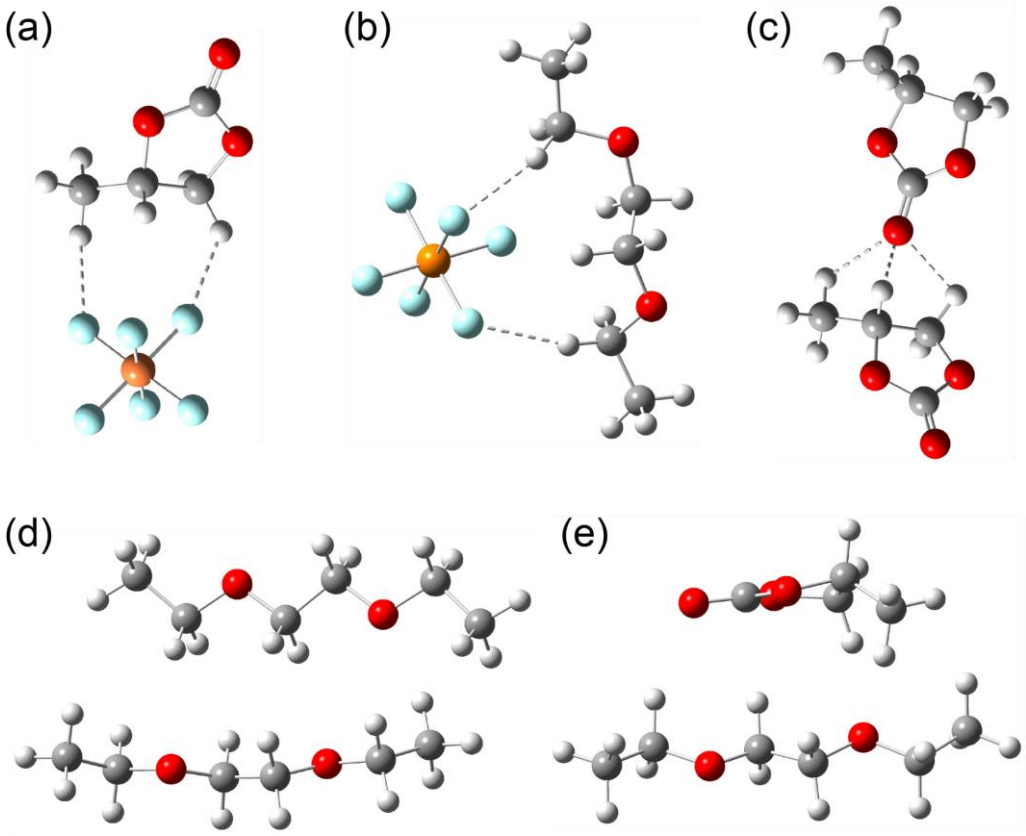

Supplementary Figure 10. The optimized structures of different complexes. (a) PC---PF_6^-. (b) DEE---PF_6^-. (c) PC---PC. (d) DEE---DEE. (e) PC---DEE. Colors of elements: H, white; C, grey; O, red; F, cyan; P, orange.

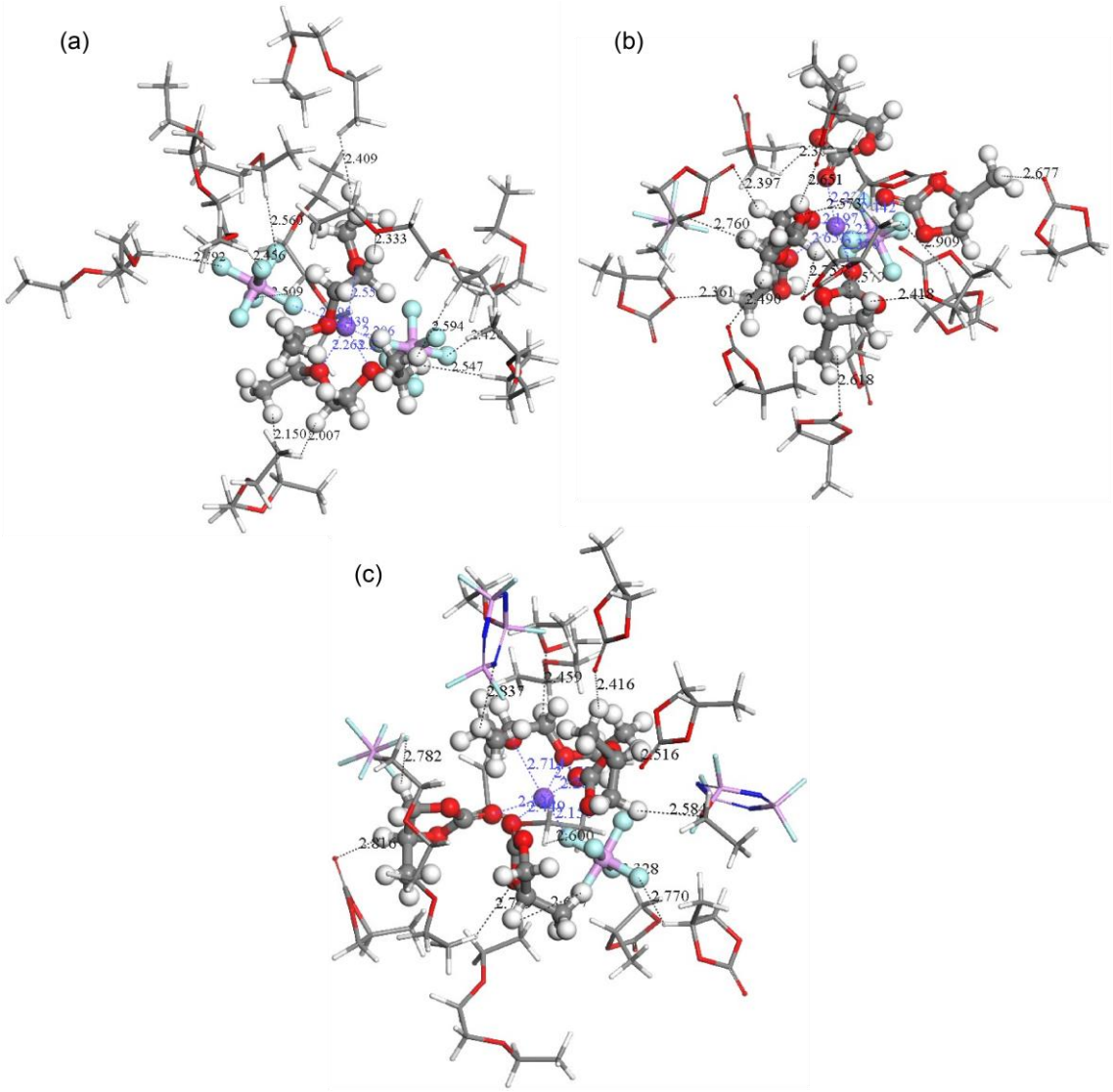

Supplementary Figure 11. The solvation structures with intricate intermolecular interactions in (a) ND, (b) NP and (c) NDPP electrolytes, respectively. Colors of elements: H, white; C, grey; N, blue; O, red; F, cyan; P, pink; Na, purple.

The intricate intermolecular interactions in the integrated solvating electrolyte NDPP have been demonstrated through molecular dynamics simulations. Apart from anion-dipole interactions between PF_6^- and PC or DEE and dipole-dipole interactions between PC and DEE, the dipolar interactions related to PFPN are also involved, which increases the disorder of the electrolyte system and diversity of solvation, facilitating ionic conductivity and the formation of uniform interfaces. Additionally, the participation of PFPN in the solvation shell further stabilizes the reactive organic solvents through dipolar interaction-mediated molecular anchoring effect, conducive to interfacial and electrochemical stability.

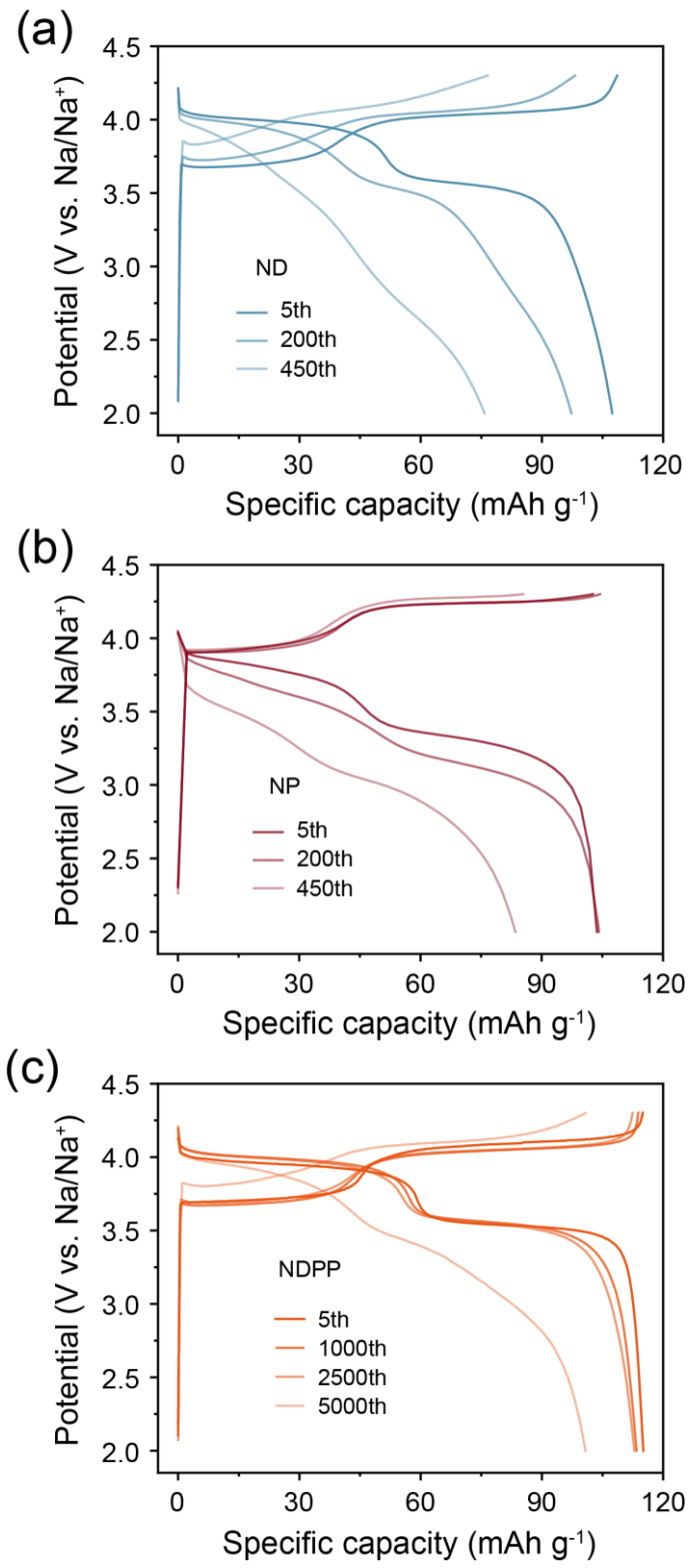

Supplementary Figure 12. Charge/discharge curves of the NVPOF positive electrode after different cycles in (a) ND, (b) NP and (c) NDPP electrolytes, respectively.

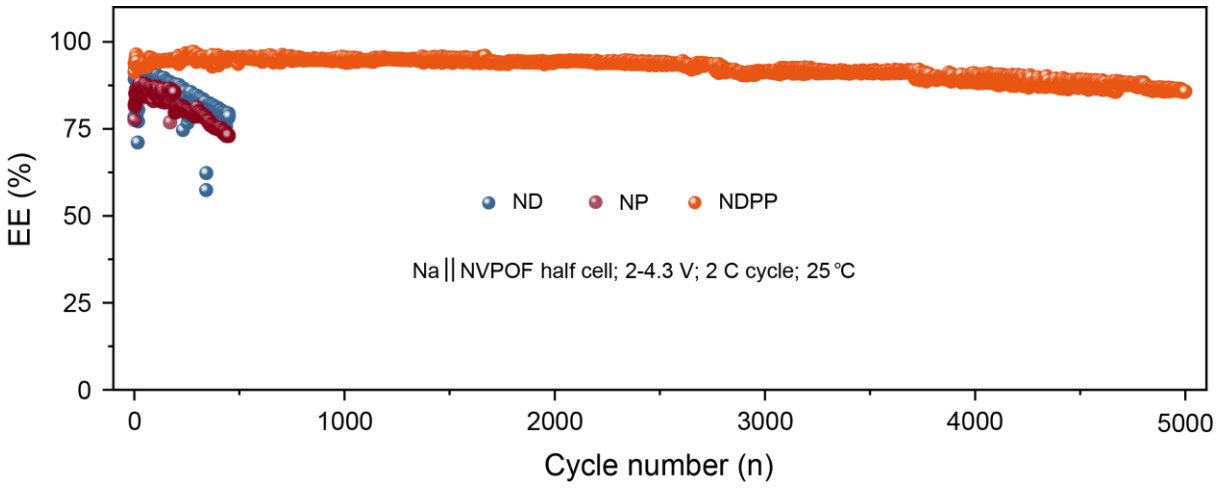

Supplementary Figure 13. The evolution of EE of Na||NVPOF half cells during the cycle.

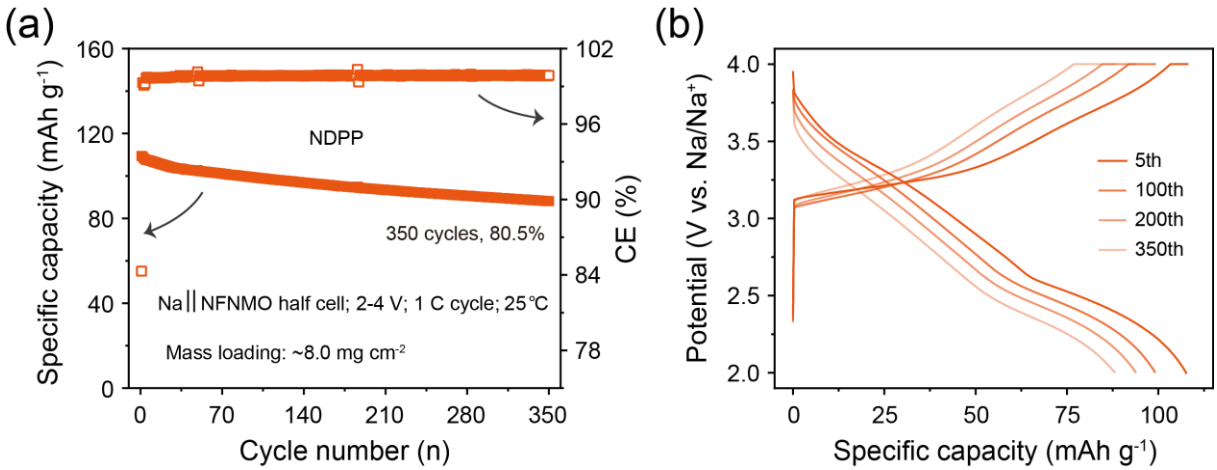

Supplementary Figure 14. (a) Cycling performance of Na||NFNMO half cells with NDPP electrolyte and (b) their GCD curves. 1 C = 120 mA g^{-1}.

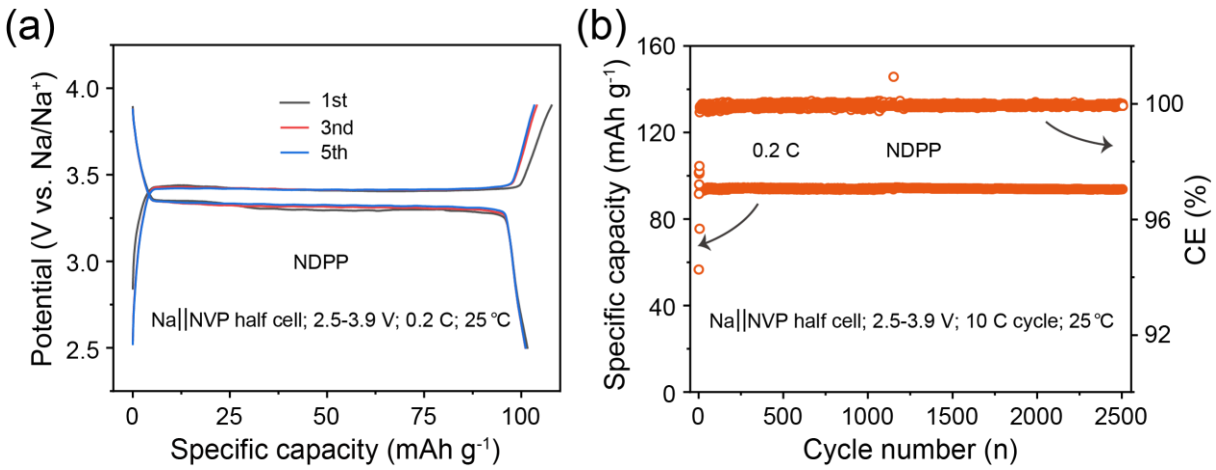

Supplementary Figure 15. Electrochemical properties of the NVP positive electrode in NDPP electrolyte at RT. (a) Typical GCD curves. (b) Cycling stability.

Supplementary Figure 16. Optical photographs of the formulated NDPP electrolyte after storage at 25, -60 and 60 ℃.

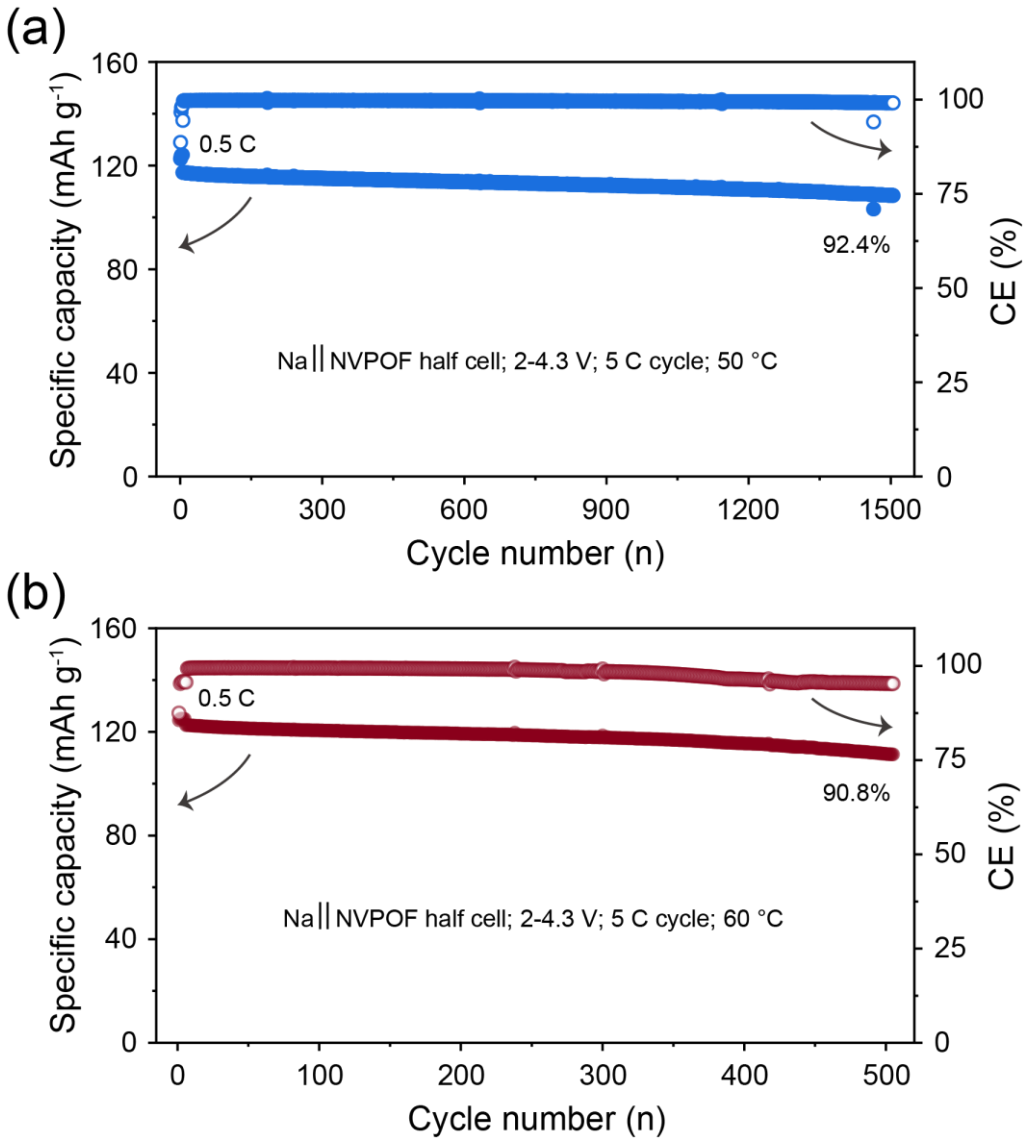

Supplementary Figure 17. Cycling stability of the NVPOF positive electrode in NDPP electrolyte at high temperatures. (a) 50 ℃. (b) 60 ℃.

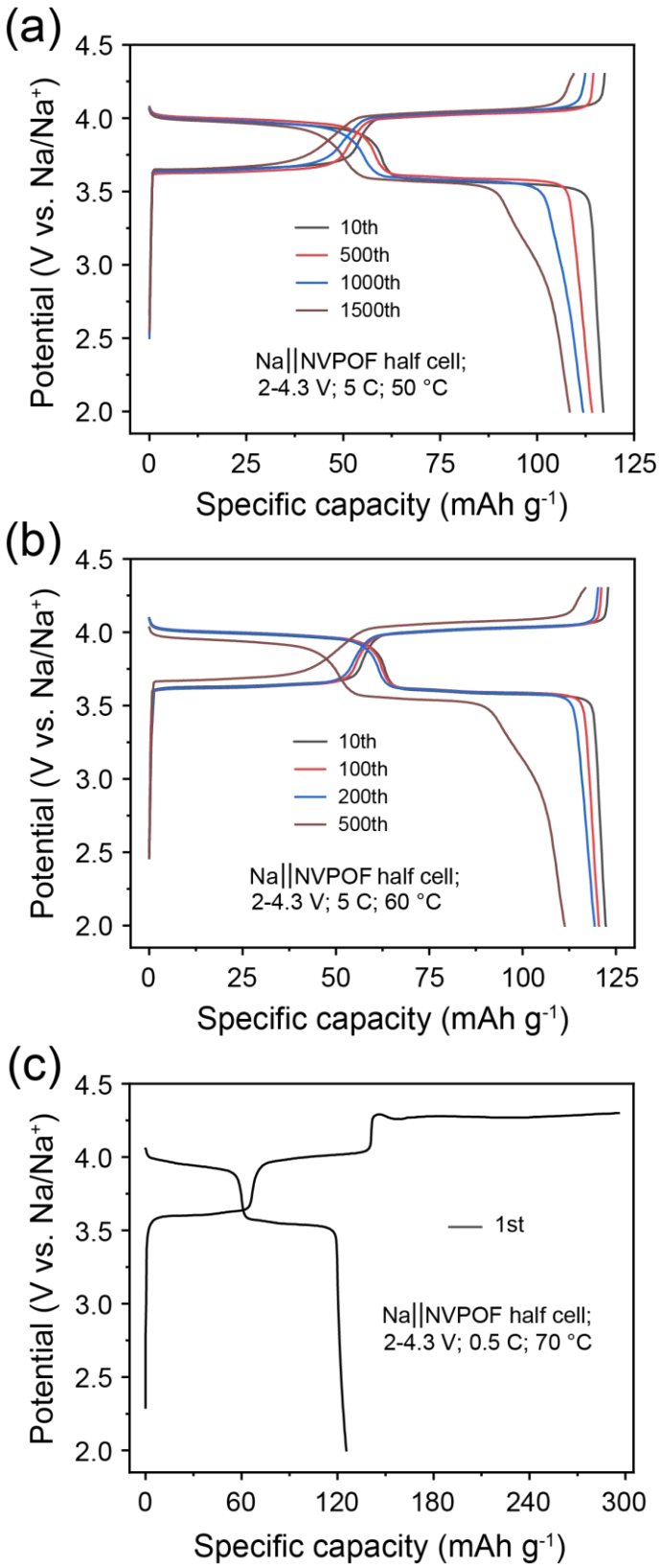

Supplementary Figure 18. GCD curves of the NVPOF positive electrode in NDPP electrolyte at high temperatures. (a) 50 ℃. (b) 60 ℃. (c) 70 ℃.

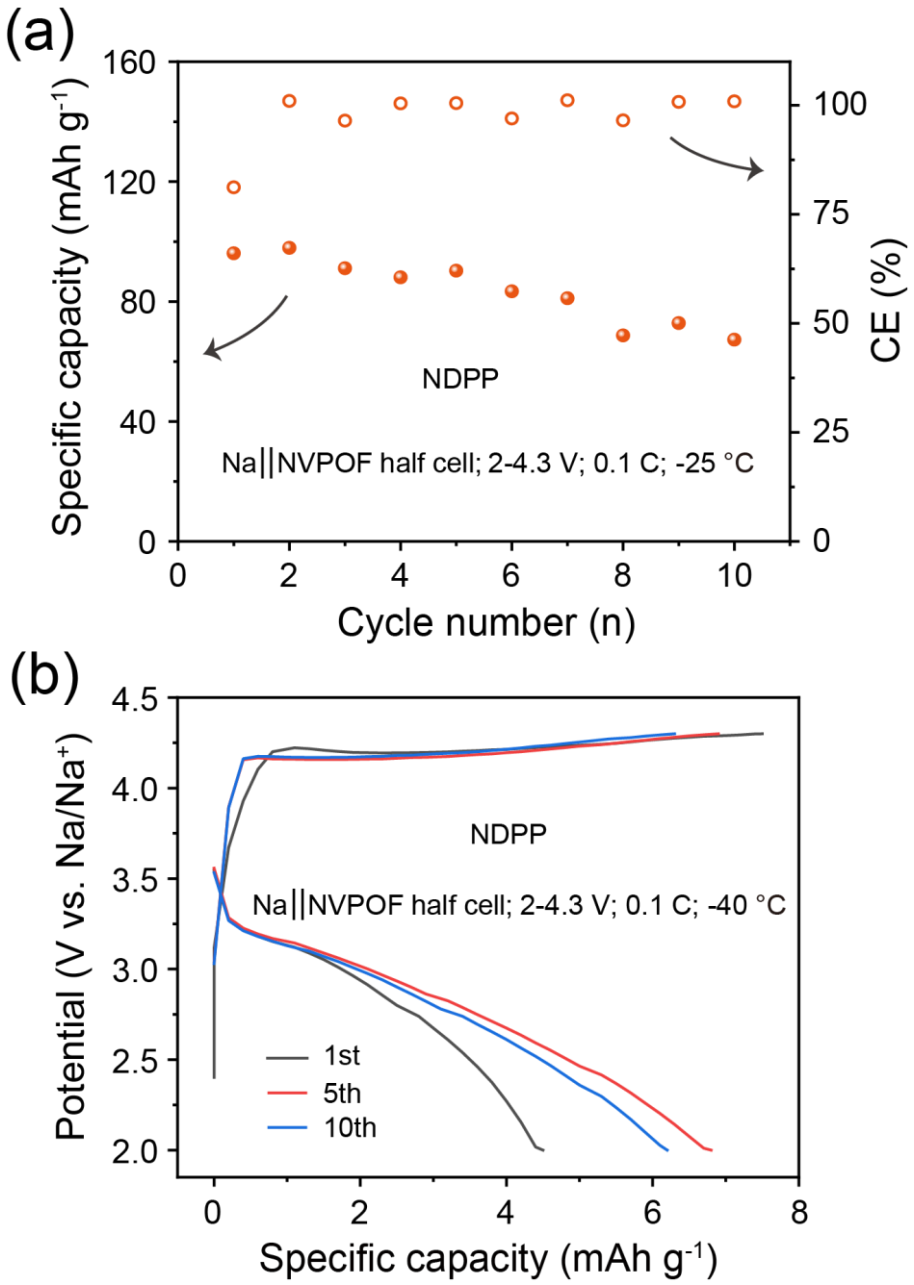

Supplementary Figure 19. Electrochemical properties of the NVPOF positive electrode in NDPP electrolyte at low temperatures. (a) Cycling stability at -25 ℃. (b) Typical GCD curves at -40 ℃.

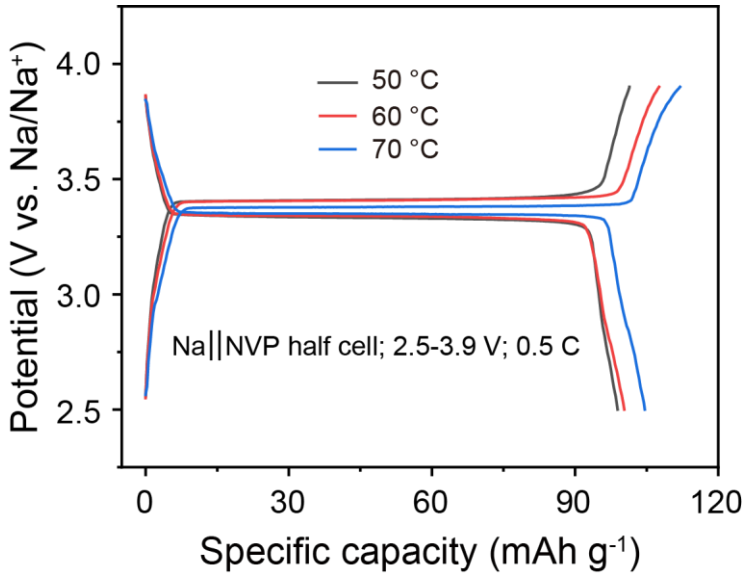

Supplementary Figure 20. Typical GCD curves of the NVP positive electrode in NDPP electrolyte at high temperatures.

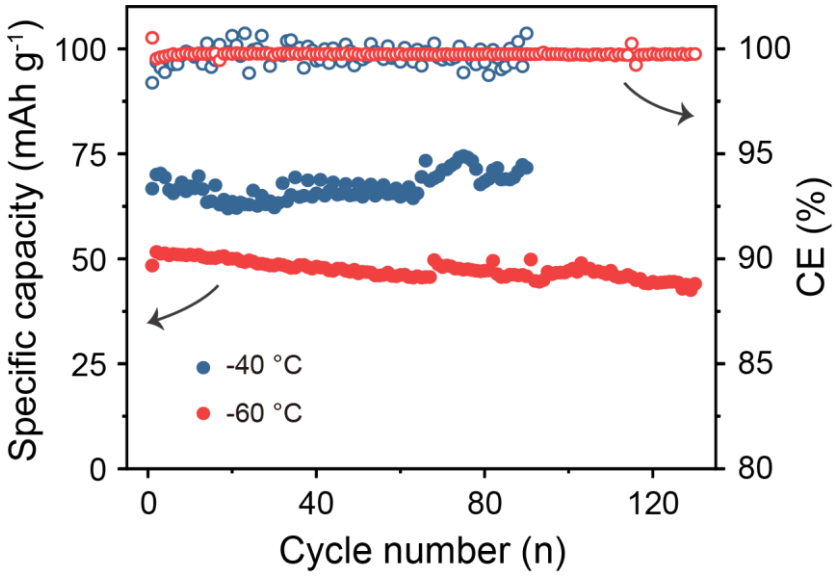

Supplementary Figure 21. Cycling stability of the NVP positive electrode in NDPP electrolyte at 0.1 C and low temperatures.

The Na^+ transportation on the negative electrode side during the charging process is mainly divided into the following steps: (i) solvated Na^+ transports in the bulk electrolyte, (ii) Na^+ de-solvation at the surface of the SEI, (iii) Na^+ migrates into the electrode across the SEI, (iv) the electrochemical reduction reaction of the electrode occurs. The relatively poor electrochemical properties at low temperatures compared to those at room temperature (e. g., reduced capacity, insufficient rate capability and lifespan) may be attributed to the sluggish ion diffusion kinetics during one or several of the above processes. The de-solvation step is considered to be the rate-determining step for the interfacial ion transfer process, demonstrating a crucial influence on the electrochemical stability.

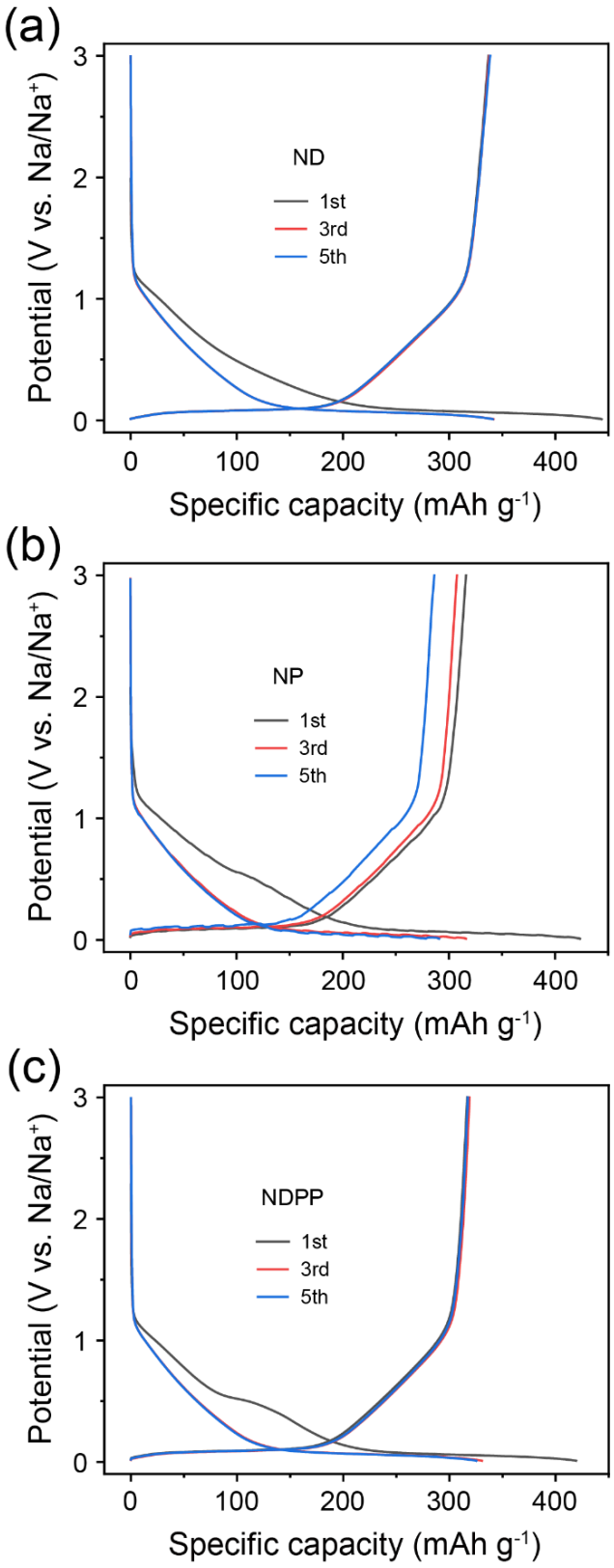

Supplementary Figure 22. GCD curves of the Na||HC half cells at 25 mA g^{-1} with different electrolytes. (a) ND, (b) NP and (c) NDPP.

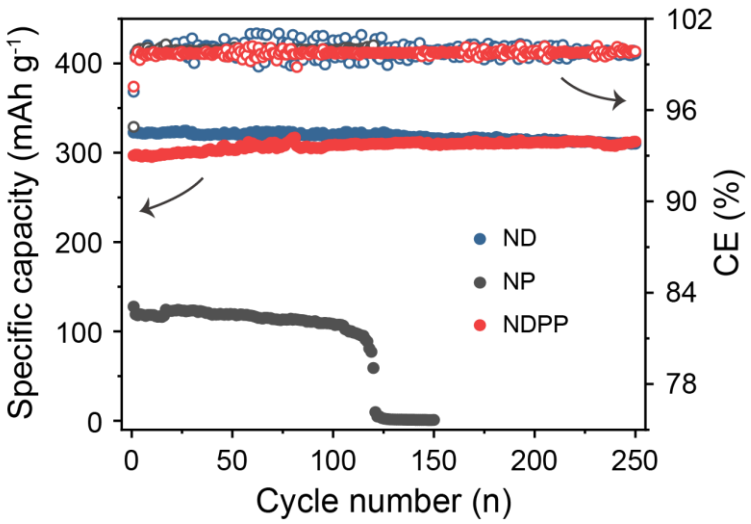

Supplementary Figure 23. Electrochemical stability of the Na||HC half cells with different electrolytes at 100 mA g^{-1}.

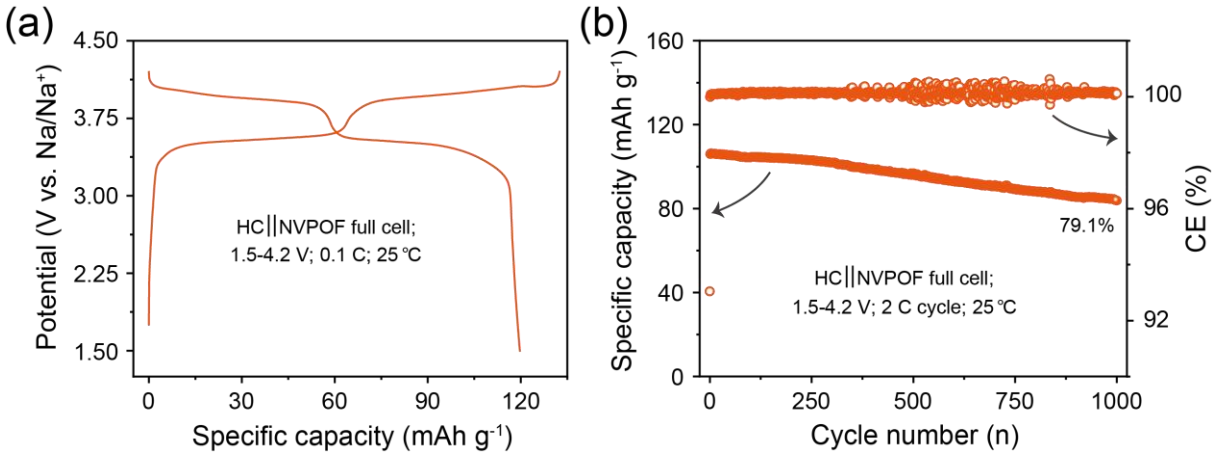

Supplementary Figure 24. Electrochemical evaluation of HC||NVPOF full cells with the NDPP electrolyte. (a) The initial GCD profile. (b) Cycling performance.

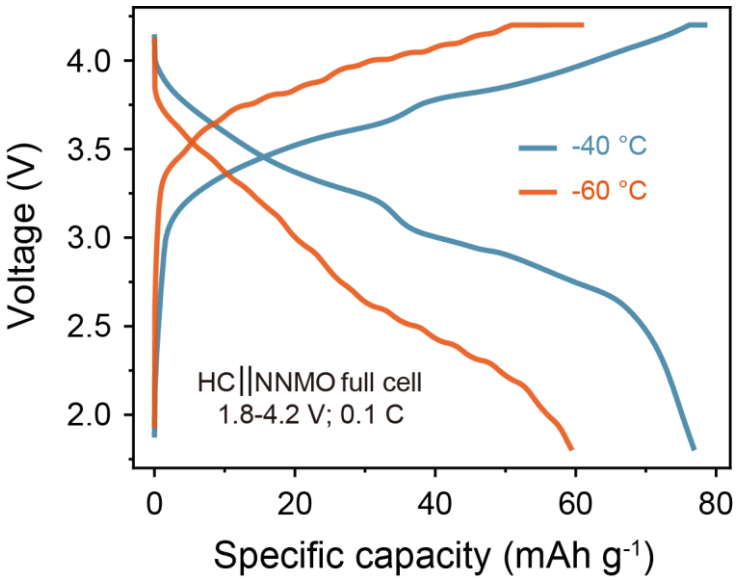

Supplementary Figure 25. The representative GCD curves of HC||NNMO full cells at 0.1 C and LTs. 1 C = 100 mA g^{-1}.

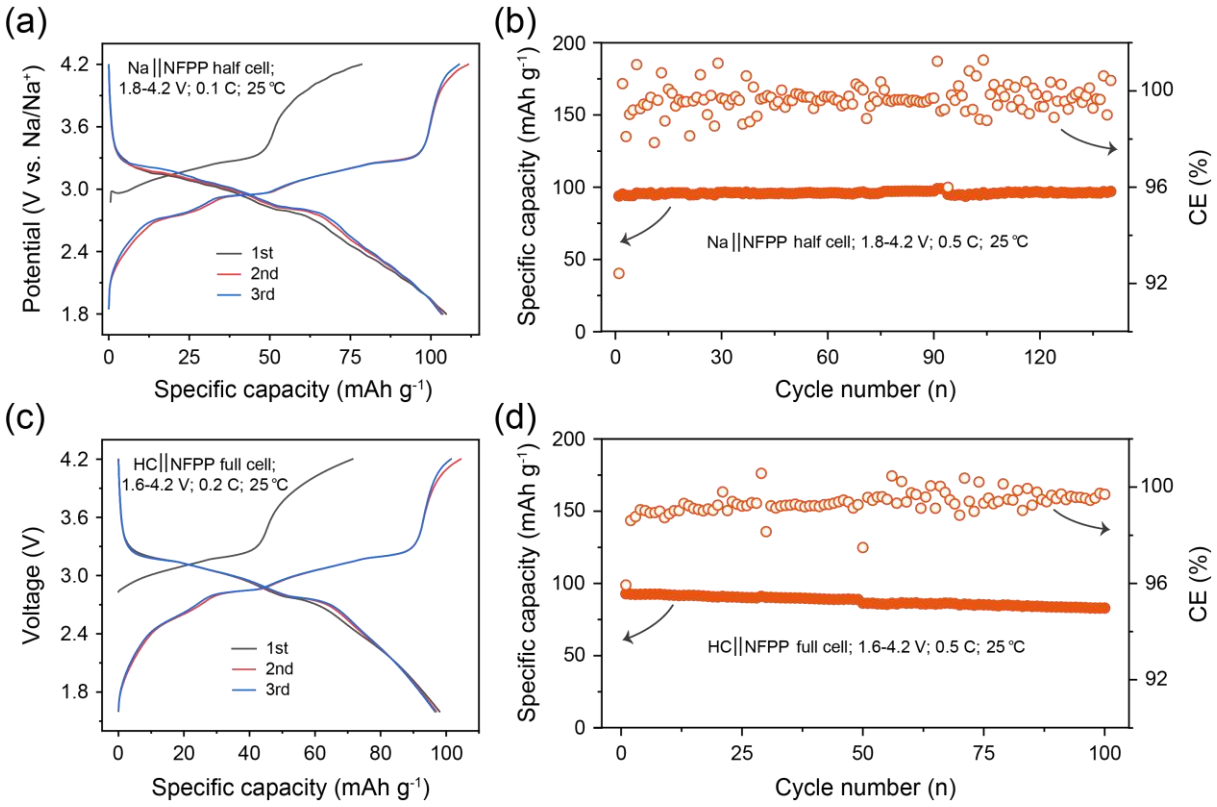

Supplementary Figure 26. Electrochemical evaluation of Na||NFPP and HC||NFPP cells with NDPP electrolyte at 25 ℃. (a) GCD curves at 0.1 C, (b) cycling performance at 0.5 C of Na||NFPP half cells. (c) GCD curves at 0.2 C, (d) cycling performance at 0.5 C of HC||NFPP full cells. 1 C = 129 mA g^{-1}.

The electrochemical stability of Na||NFPP and HC||NFPP cells with NDPP electrolyte was investigated at 25 ℃. Specifically, Na||NFPP half cells demonstrated the initial reversible specific capacity of ~104 mAh g^{-1} at 0.1 C and stable cycling performance at 0.5 C and 1.8-4.2 V. For the HC||NFPP full cells, there were ~97 mAh g^{-1} of discharge specific capacity at 0.2 C and ~89.3% of capacity retention over 100 cycles at 0.5 C and 1.6-4.2 V.

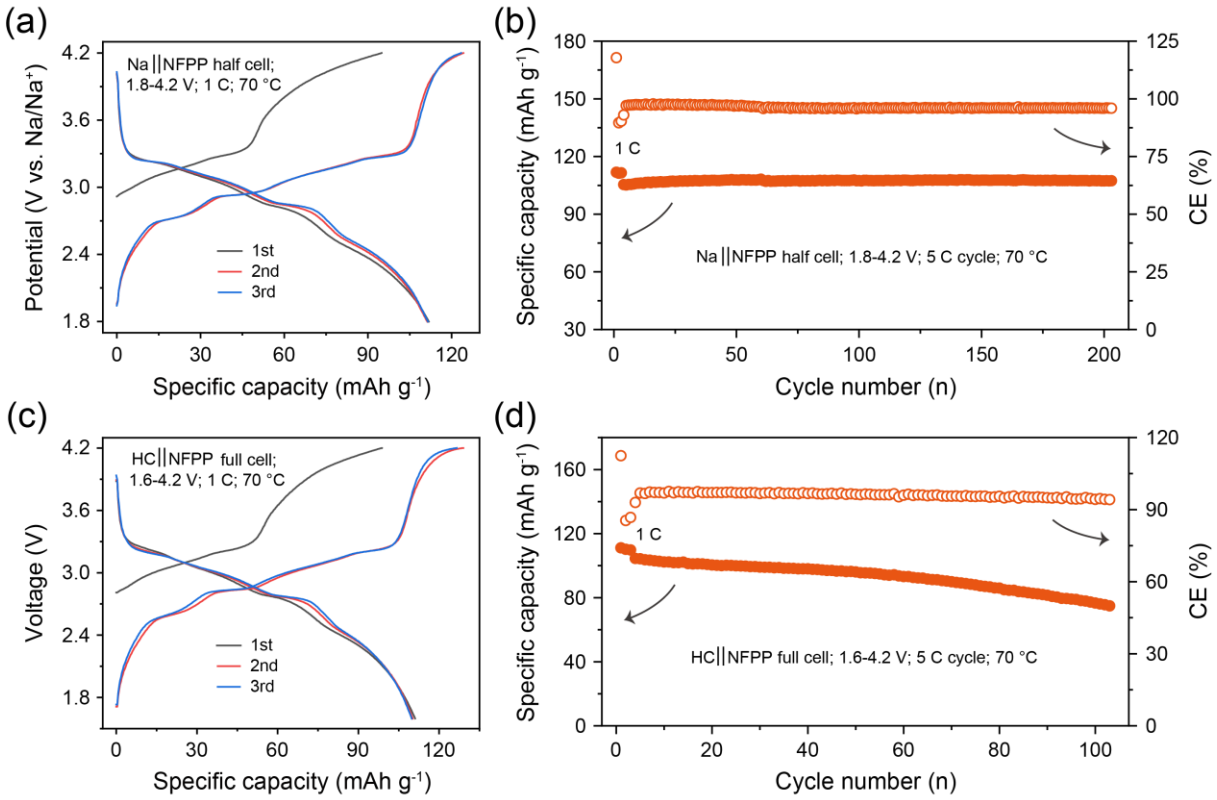

Supplementary Figure 27. Electrochemical evaluation of Na||NFPP and HC||NFPP cells with NDPP electrolyte at 70 ℃. (a) GCD curves at 1 C, (b) cycling performance at 5 C of Na||NFPP half cells. (c) GCD curves at 1 C, (d) cycling performance at 5 C of HC||NFPP full cells.

To substantiate the high-temperature stability, we have further carried out the electrochemical evaluation of Na||NFPP and HC||NFPP cells with NDPP electrolyte at 70 ℃. Specifically, Na||NFPP half cells demonstrated the stable reversible capacity of ~107 mAh g^{-1} over 200 cycles at a 5 C rate and within a voltage range of 1.8 to 4.2 V. For the HC||NFPP full cells, there was a capacity retention of 71.7% during the 100-cycle process at a 5 C rate and within a voltage range of 1.6 to 4.2 V.

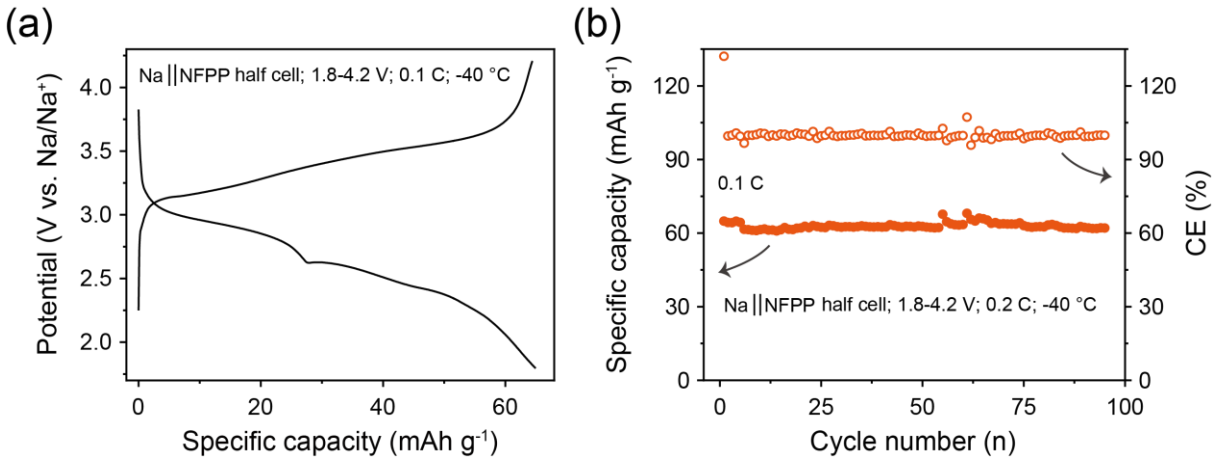

Supplementary Figure 28. Electrochemical evaluation of Na||NFPP half cells with NDPP electrolyte at -40 ℃. (a) The typical GCD curve. (b) Cycling stability.

Furthermore, the Na||NFPP half cells with NDPP electrolyte can deliver approximately 65 mAh g^{-1} of reversible capacity at 0.1 C and -40 ℃. Meanwhile, stable cycles can be observed at 0.2 C and -40 ℃.

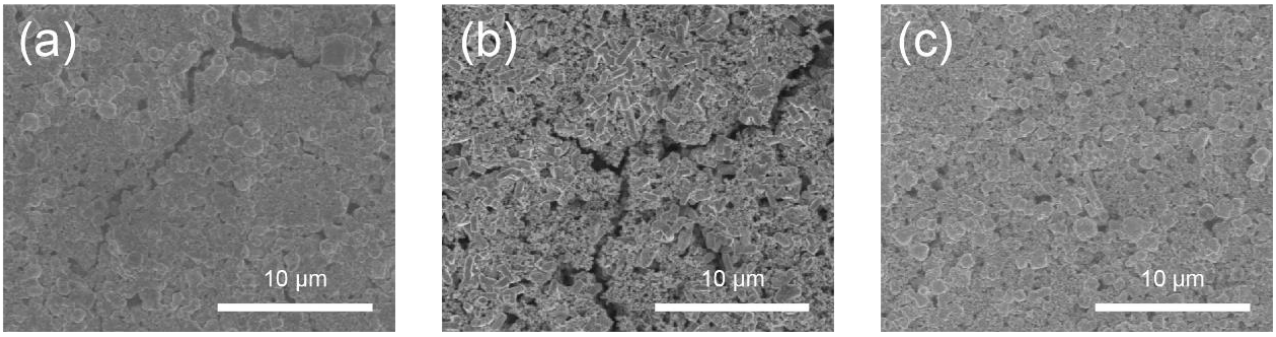

Supplementary Figure 29. SEM images for the NVPOF positive electrodes after 50 cycles at 0.5 C and 25 ℃. (a) ND, (b) NP and (c) NDPP electrolytes, respectively.

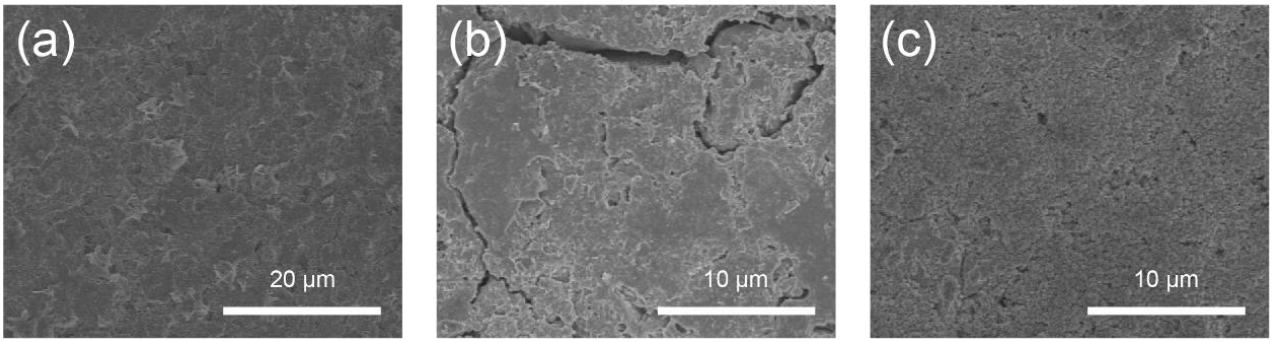

Supplementary Figure 30. SEM images of the HC negative electrodes after 50 cycles at 50 mA g^{-1} and 25 ℃. (a) ND, (b) NP and (c) NDPP electrolytes, respectively.

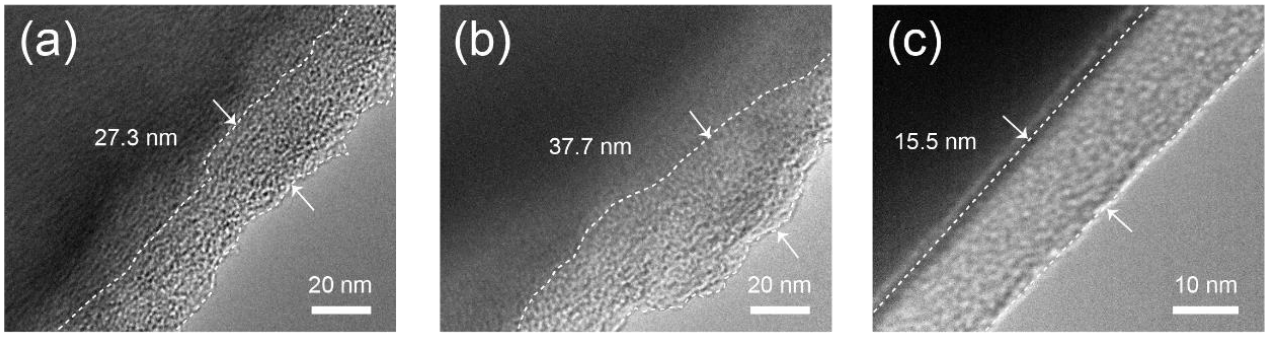

Supplementary Figure 31. TEM images for the HC negative electrodes after 50 cycles at 50 mA g^{-1} and 25 ℃. (a) NDPP, (b) NP and (c) ND electrolytes, respectively.

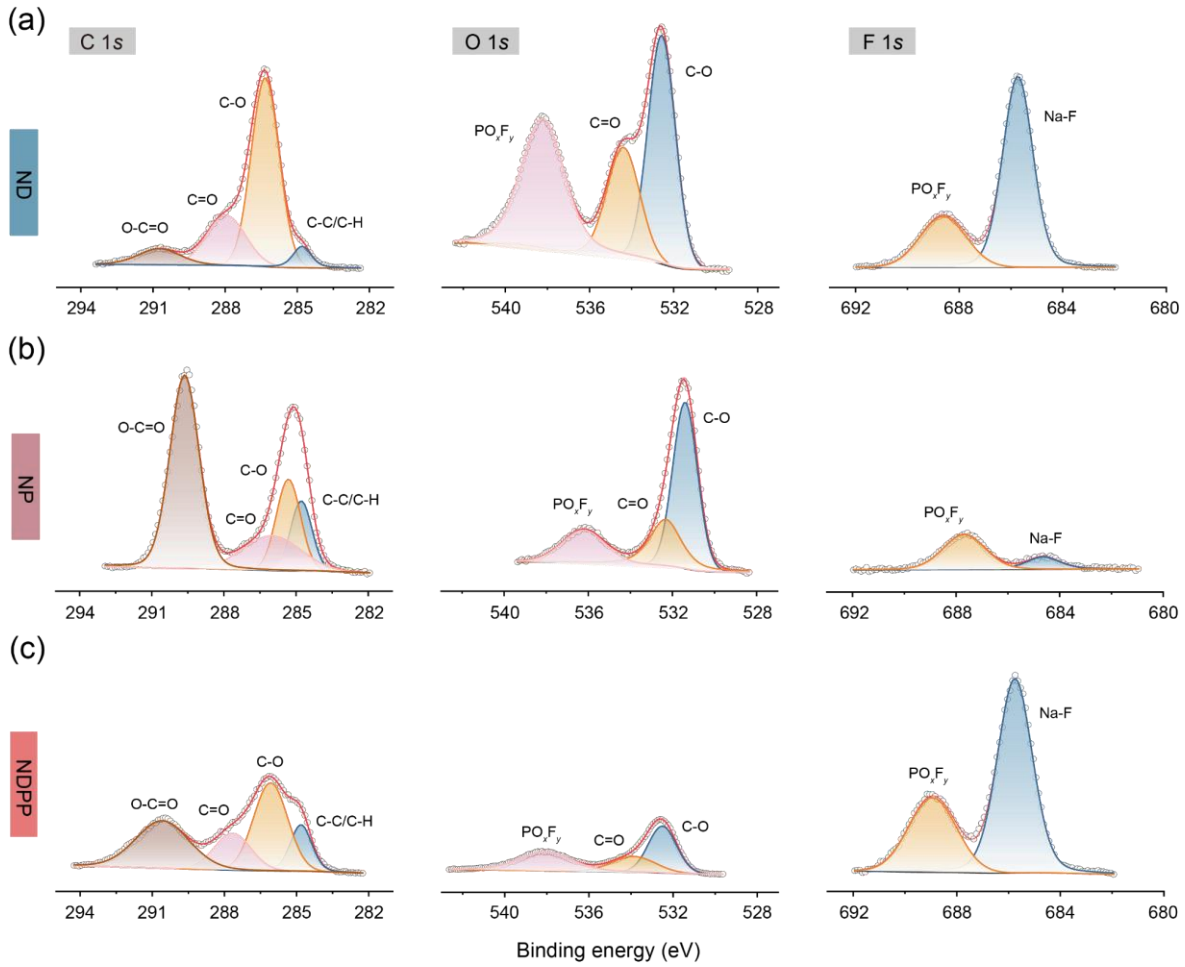

Supplementary Figure 32. XPS spectra for C 1*s*, O 1*s* and F 1*s* for the HC negative electrodes after 50 cycles at 50 mA g^{-1} and 25 ℃. (a) ND, (b) NP and (c) NDPP electrolytes, respectively.

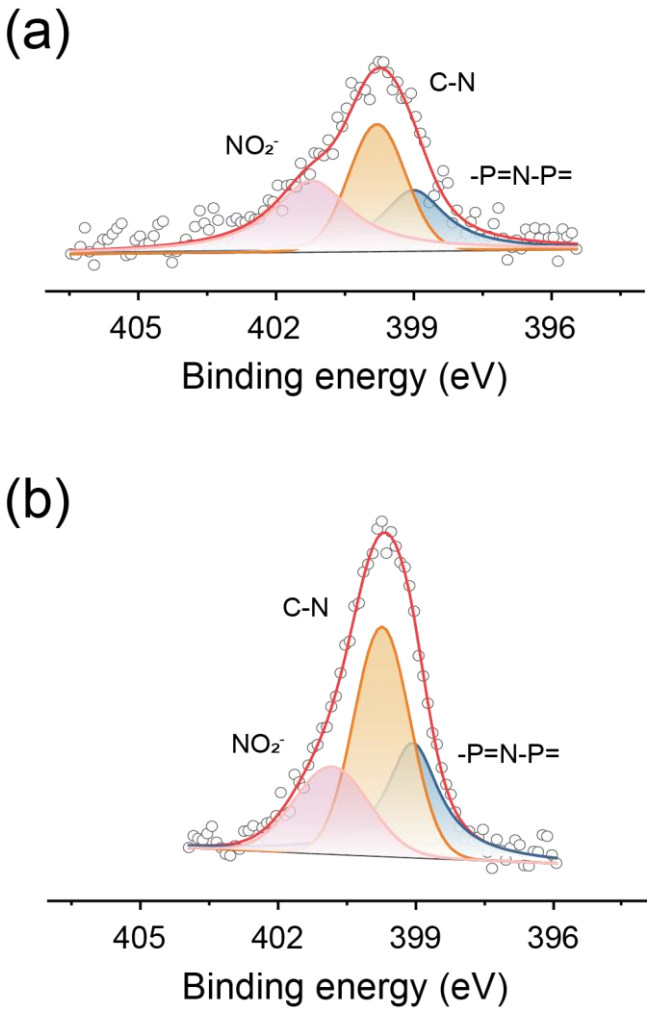

Supplementary Figure 33. XPS spectra for N 1*s* for the cycled (a) NVPOF and (b) HC electrodes in NDPP, respectively.

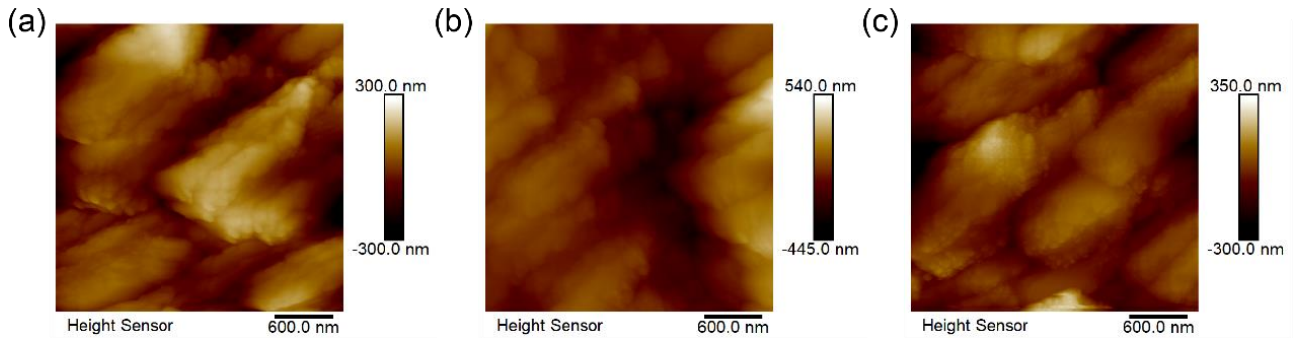

Supplementary Figure 34. 2 D AFM images for the cycled NVPOF positive electrodes in (a) ND, (b) NP and (c) NDPP electrolytes, respectively.

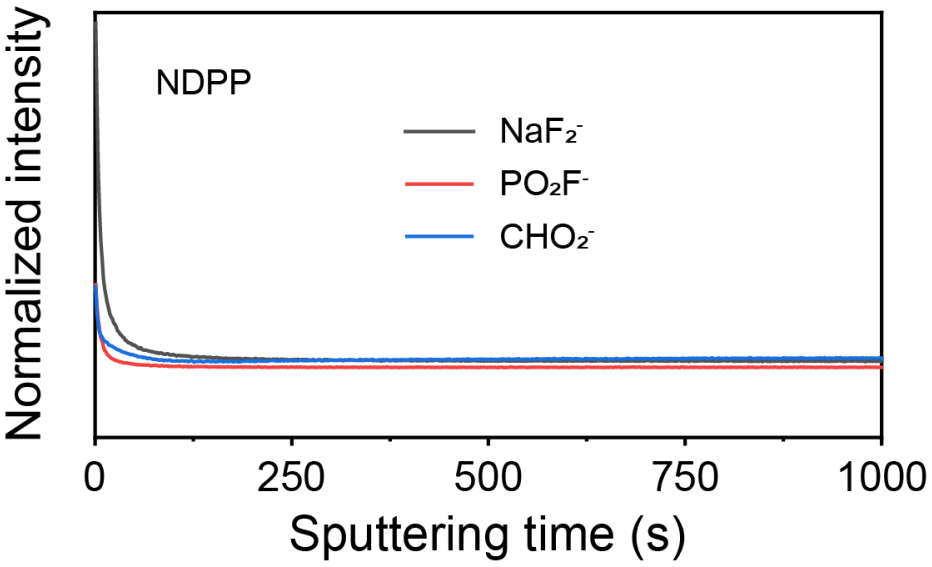

Supplementary Figure 35. TOF-SIMS depth profiles of the ion fragments on the NVPOF positive electrode after 50 cycles at 0.5 C and 25 ℃ in NDPP electrolyte.

Supplementary Table 1: Abbreviations of different solvents.

Name	Abbreviations
Ethylene carbonate	EC
Propylene carbonate	PC
Dimethyl carbonate	DMC
Diethyl carbonate	DEC
Ethyl methyl carbonate	EMC
1,2-Dimethoxyethane	DME
Diethylene glycol dimethyl ether	G2
Ethylene glycol diethyl ether	DEE
Tetrahydrofuran	THF
2-Methyltetrahydrofuran	MeTHF
Tetrahydropyran	THP
Ethoxy (pentafluoro)cyclotriphosphazene	PFPN

Supplementary Table 2: A series of basic physicochemical properties of various solvents.

Solvent	Melting point (T_m) [℃]	Boiling point (T_b) [℃]	Flash point (T_f) [℃]	Viscosity (η) at 25 ℃ [cP]	Dielectric constant (ε) at 25 ℃	DN value
EC	36.4	248	160	1.9	89.78	16.4
PC	-48.8	242	132	2.53	64.9	15.1
DMC	4.6	91	18	0.59	3.11	16
DEC	-74.3	126	31	0.75	2.81	16
EMC	-53	110	23	0.65	2.4	17.2
DME	-58	82.5	0	0.45	7.18	20
G2	-64	162	57	1.88	7.23	19.5
DEE	-74	121	27	-	3.9	-
THF	-108.5	66	-14	0.46	7.58	20
MeTHF	-137.2	78	-11	0.47	6.97	18
THP	-45.2	87.9	-15.6	0.764	5.61	22

Supplementary Table 3: Names and formulae of the studied electrolyte systems.

Name	Composition
ND	0.8 M $NaPF_6$ in DEE
NP	0.8 M $NaPF_6$ in PC
NDP	0.8 M $NaPF_6$ in DEE-PC (1: 1 by volume ratio)
NDPP	0.8 M $NaPF_6$ in DEE-PC-PFPN (5: 5: 2 by volume ratio)

Supplementary Table 4: Recent advances in the electrochemical stability of various NVPOF-based full cells.

Configuration description	Specific current	Cycling number, retention	Ref.
HC||$Na_3V_{1.85}Fe_{0.15}(PO_4)_2O_2F$	0.4 C	100, 82.3%	1
HC||NVOPF	1 C	500, ~80%	2
SbSn/NPC||$Na_3V_2(PO_4)_{1.95}(SO_4)_{0.05}O_2F$	3 C	100, 75.0%	3
a-Se||NVPOF-$Zn_{0.05}$	10 C	900, 77.6%	4
HC||$N(VO)_{1.8}Fe_{0.2}PF_{1.2}$	500 mA g^{-1}	200, 94.7%	5
HC||$Na_{3-y}VPO_{2-x}Br_xF$	5 C	1000, 84.9%	6
HC||NVPOF-HE	5 C	1000, ~93.8%	7
HC||NVOPF-PE	3 C	750, ~91%	8
HC||NVPOF	**0.2 C** **2 C**	**80, 98.5%** **1000, 79.1%**	**This work**

Supplementary Table 5: The fabrication parameters of 1 Ah HC||NNFMO pouch cells.

Cell capacity (Ah)	1	
Cell weight (g)	38.0	
Specific energy (Wh kg^{-1})	102.8	
Positive electrode	Active material	NaNiFeMnO
	Active material percentage (wt%)	95.3
	Area weight (each side, mg cm^{-2})	20.0
	Area capacity (each side, mAh cm^{-2})	1.93
	Length (mm)	80
	Width (mm)	60
	Thickness (μm)	140
	Compact density (g cm^{-3})	3
Negative electrode	Active material	Hard carbon
	Active material percentage (wt%)	94.5
	Area weight (each side, mg cm^{-2})	8.0
	Area capacity (each side, mAh cm^{-2})	2.12
	Length (mm)	84
	Width (mm)	64
	Thickness (μm)	170
	Compact density (g cm^{-3})	0.97
Layer of positive electrodes	8	
Layer of negative electrodes	9	
Negative to positive capacity ratio		1.1
Thickness of separator (μm)		12
Thickness of packing foil (μm)		113
Electrolyte to capacity ratio (g Ah^{-1})		5

Supplementary References

1. Yue L, *et al.* $Na_3V_{2-x}Fe_x(PO_4)_2O_2F$: An advanced cathode material with ultra-high stability for superior sodium storage. *Chem Eng J* **441**, 136132 (2022).
2. Liu Y, *et al.* Electrolyte Engineering with Tamed Electrode Interphases for High-Voltage Sodium-Ion Batteries. *Adv Mater* **36**, 2310051 (2024).
3. Wang X, *et al.* Rational modulation of fluorophosphate cathode by anionic groups to reduce the polarization behavior for fast-charging sodium-ion batteries. *J Energy Chem* **100**, 509-521 (2025).
4. Yu H, *et al.* Unlocking the Sodium Storage Potential in Fluorophosphate Cathodes: Electrostatic Interaction Lowering Versus Structural Disordering. *Adv Mater* **37**, 2400229 (2025).
5. Fu Q, *et al.* Activating reversible multi-electron reaction of $Na_3(VO)_2(PO_4)_2F$ cathode via Fe/F dual-doping for high-energy and stable sodium storage. *Energy Storage Mater* **74**, 103960 (2025).
6. Wang J, *et al.* Electrostatically Shielded Transportation Enabling Accelerated Na^+ Diffusivity in High-Performance Fluorophosphate Cathode for Sodium-Ion Batteries. *Adv Funct Mater* **34**, 2315318 (2024).
7. Su G, *et al.* Insights into Tiny High-Entropy Doping Promising Efficient Sodium Storage of $Na_3V_2(PO_4)_2O_2F$ toward Sodium-Ion Batteries. *Adv Energy Mater* **15**, 2403282 (2025).
8. Xu C, *et al.* Overcoming Kinetic Limitations of Polyanionic Cathode toward High-Performance Na-Ion Batteries. *ACS Nano* **18**, 18758-18768 (2024).